Compendium of Current Single Event Effects Results from NASA Goddard Space Flight Center and NASA Electronic Parts and Packaging Program

Martha V. O'Bryan[1], Kenneth A. LaBel[2], Edward P. Wilcox[1], Dakai Chen[3], Michael J. Campola[2], Megan C. Casey[2], Jean-Marie Lauenstein[2], Edward J. Wyrwas[4], Steven M. Guertin[5], Jonathan A. Pellish[2], and Melanie D. Berg[1]

1. AS&D, Inc.; 2. NASA GSFC; 3. Analog Devices Inc. (formerly with NASA GSFC); 4. Lentech, Inc.; 5. JPL

Martha O'Bryan

National Aeronautics and Space Administration

Abstract: We present the results of single event effects (SEE) testing and analysis investigating the effects of radiation on electronics. This paper is a summary of test results.

Introduction

NASA spacecraft are subjected to a harsh space environment that includes exposure to various types of ionizing radiation. The performance of electronic devices in a space radiation environment are often limited by their susceptibility to single event effects (SEE). Ground-based testing is used to evaluate candidate spacecraft electronics to determine risk to spaceflight applications. Interpreting the results of radiation testing of complex devices is challenging. Given the rapidly changing nature of technology, radiation test data are most often application-specific and adequate understanding of the test conditions is critical.

Studies discussed herein were undertaken to establish the application-specific sensitivities of candidate spacecraft and emerging electronic devices to single-event upset (SEU), single-event latchup (SEL), single-event gate rupture (SEGR), single-event burnout (SEB), and single-event transient (SET).

For total ionizing dose (TID) results, see a companion paper submitted to the 2017 Institute of Electrical and Electronics Engineers (IEEE) Nuclear and Space Radiation Effects Conference (NSREC) Radiation Effects Data Workshop (REDW) entitled "Compendium of Current Total Ionizing Dose and Displacement Damage Results from NASA Goddard Space Flight Center and Selected NASA Electronic Parts and Packaging Program" by A. D. Topper, et al.

Test Techniques and Setup

A. Test Facilities

All tests were performed between February 2016 and February 2017. Heavy ion experiments were conducted at the Lawrence Berkeley National Laboratory (LBNL) 88-inch cyclotron [3], and at the Texas A&M University Cyclotron (TAMU) [4]. Both of these facilities provide a variety of ions over a range of energies for testing. Each device under test (DUT) was irradiated with heavy ions having linear energy transfer (LET) ranging from 0.07 to 86 MeV•cm²/mg. Fluxes ranged from 1×10^2 to 1×10^5 particles/cm²/s, depending on device sensitivity. Representative ions used are listed in Tables I, and II. LETs in addition to the values listed were obtained by changing the angle of incidence of the ion beam with respect to the DUT, thus changing the path length of the ion through the DUT and the "effective LET" of the ion. Energies and LETs available varied slightly from one test date to another.

Proton SEE tests were performed University of California at Davis (UCD) Crocker Nuclear Laboratory (CNL) using a 76" cyclotron (maximum energy of 63 MeV) [5] and Mass General Hospital (MGH) Francis H. Burr Proton Therapy.

Laser SEE tests were performed at the pulsed laser facility at the Naval Research Laboratory (NRL) We tested with a pulsed laser at the Naval Research Laboratory using both Single-Photon Absorption (SPA) and Two-Photon Absorption (TPA) techniques with the laser light having a wavelength of 590 nm resulting in a skin depth (depth at which the light intensity decreased to 1/e – or about 37% – of its intensity at the surface) of 2 µm. A nominal pulse rate of 1 kHz was utilized. Pulse width was 1 ps, beam spot size ~1.2 µm.

Table I: LBNL Test Heavy Ions

Ion	Energy (MeV)	Surface LET in Si (MeV•cm²/mg) (Normal Incidence)	Range in Si (µm)
LBNL 10 MeV per amu tune			
^{13}C	183	2.2	226
^{21}Ne	216	3.5	175
^{40}Ar	400	9.7	130
^{51}V	508	14.6	113
^{63}Cu	660	21.2	108
^{86}Kr	906	30.2	113
^{107}Ag	1039	48.2	90
^{124}Xe	1233	58.8	90

Table II: TAMU Test Heavy Ions

Ion	Energy (MeV)	Surface LET in Si (MeV•cm²/mg) (Normal Incidence)	Range in Si (µm)
TAMU 15 MeV per amu tune			
^{14}N	210	1.3	428
^{20}Ne	300	2.5	316
^{40}Ar	599	7.7	229
^{63}Cu	944	17.8	172
^{84}Kr	1259	25.4	170
^{109}Ag	1634	38.5	156
^{129}Xe	1934	47.3	156
^{197}Au	2954	80.2	155
TAMU 25 MeV per amu tune			
^{86}Kr	2081	19.8	332
^{136}Xe	3197	38.9	286

amu = atomic mass unit

B. Test Method

Unless otherwise noted, all tests were performed at room temperature and with nominal power supply voltages. Device qualification include SEL high-temperature, V_{CC} plus worst-case and for SEU/SET high-temperature, V_{CC} minus worst-case. Unless otherwise noted, SEE testing was performed in accordance with JESD57 test procedures where applicable.

1) SEE Testing - Heavy Ion:

Depending on the DUT and the test objectives, one or more of three SEE test approaches were typically used:

Dynamic – the DUT was continually exercised while being exposed to the beam. The events and/or bit errors were counted, generally by capturing with a high-speed oscilloscope, digital input/output (DIO) device, microprocessor, FPGA, or by comparing the DUT output to an unirradiated reference device or with an expected output (Golden chip or virtual Golden chip methods). In some cases, the effects of clock speed or device operating modes were investigated. *Results of such tests should be applied with caution due to their application-specific nature.*

Static – the DUT was configured prior to irradiation; data were retrieved and errors were counted after irradiation.

Biased – the DUT was biased and clocked while power consumption was monitored for SEL or other destructive effects. In most SEL tests, functionality was also monitored.

In SEE experiments, DUTs were monitored for soft errors, such as SEUs, and for hard errors, such as SEGR. Detailed descriptions of the types of errors observed are noted in the individual test reports on radhome.nasa.gov and nepp.nasa.gov.

SET testing was performed using high-speed oscilloscopes controlled via National Instruments LabVIEW®. Individual criteria for SETs are specific to the device and application being tested.

Heavy ion SEE sensitivity experiments include measurement of the linear energy transfer threshold (LET_{th}) and cross section at the maximum measured LET. The LET_{th} is defined as the maximum LET value at which no effect was observed at an effective fluence of 1×10^7 particles/cm². In the case where events are observed at the smallest LET tested, LET_{th} will either be reported as less than the lowest measured LET or determined approximately as the LET_{th} parameter from a Weibull fit. In the case of SEGR and SEB experiments, measurements are made of the SEGR or SEB threshold V_{DS} (drain-to-source voltage) as a function of LET and ion energy at a fixed V_{GS} (gate-to-source voltage).

2) SEE Testing - Proton:

Proton SEE tests were performed in a manner similar to heavy ion exposures. However, because protons usually cause SEE via indirect ionization of recoil particles, results are parameterized in terms of proton energy rather than LET. Because such proton-induced nuclear interactions are rare, proton tests also feature higher cumulative fluences and particle flux rates than heavy ion experiments.

3) SEE Testing - Pulsed Laser Facility Testing:

The DUT was mounted on an X-Y-Z stage in front of a 100x lens that produces a spot diameter of approximately 1 µm at full-width half-maximum (FWHM). The X-Y-Z stage can be moved in steps of 0.1 µm for accurate determination of SEE-sensitive regions in front of the focused beam. An illuminator, together with a charge-coupled device (CCD) camera and monitor, were used to image the area of interest thereby facilitating accurate positioning of the device in the beam. The pulse energy was varied in a continuous manner using a polarizer/half-waveplate combination and the energy was monitored by splitting off a portion of the beam and directing it at a calibrated energy meter.

Test Results Overview

Principal investigators are listed in Table III. Abbreviations and conven-tions are listed in Table IV. SEE results are summarized in Table V. Unless otherwise noted all LETs are in MeV•cm²/mg and all cross sections are in cm²/device. All SEL tests are performed to a fluence of 1×10^7 particles/cm². Proton tests were performed at a flux rate of 1×10^7 to 1×10^8 p⁺/cm²-s. The fluence was to until an event (upset was observed, or 1×10^{10} to 1×10^{11} p⁺/cm²) or per at a given energy (i.e. 200 MeV, etc).

Table III: List of Principal Investigators

Principal Investigator (PI)	Abbreviation
Melanie D. Berg	MB
Megan C. Casey	MCC
Michael J. Campola	MJC
Dakai Chen	DC
Steve Guertin	SG
Jean-Marie Lauenstein	JML
Edward (Ted) P. Wilcox	TW
Edward Wyrwas	EW

Table IV: Abbreviations and Conventions

LET_i = linear energy transfer (MeV•cm²/mg)
LET_{th} = linear energy transfer threshold (the maximum LET value at which no effect was observed at an effective fluence of 1×10^7 particles/cm²) – in MeV•cm²/mg)
LET_{SEC} = LET for SIC
< = SEE observed at lowest tested LET
> = no SEE observed at highest tested LET
σ = cross section (cm²/device, unless specified as cm²/bit)
$\sigma_{saturation}$ = cross section at maximum measured LET (cm²/device, unless specified as cm²/bit)
ADC = analog-to-digital converter
Codec = codec/decodec
CMOS = complementary metal oxide semiconductor
DDR = double data rate
DUT = device under test
ECC = error correcting code
Effective LET = the ion LET divided by the cosine of the angle of incidence
H = heavy ion test
ID# = identification number
I_d = drain-source
I_{dss} = drain-source leakage current
I_{out} = output current
L = laser test
LBNL = Lawrence Berkeley National Laboratory
LDC = lot date code
LPP = low power plus
MLC = multi-level cell
n/a = not available
NRL = Naval Research Laboratory
PI = principal investigator
PIN Diode = diode with p-type semiconductor and an n-type semiconductor region
REAG = radiation effects and analysis group
SBU = single-bit upset
SEB = single event burnout
SEE = single event effect
SEGR = single event gate rupture
SEL = single event latch-up
SET = single event transient
SEU = single event upset
SLC = Single-level cell
SOC = system on chip
TAMU = Texas A&M University Cyclotron Facility
V_{DS} = drain-source voltage
V_{GS} = gate-source voltage
V_{th} = gate threshold voltage

Table V: Summary of SEE Test Results

Part Number	Manufacturer	LDC or Wafer#, (REAG ID#)	Device Function	Technology	Particle: (Facility\Year/Month) P.I.	Test Results: LET in MeV•cm²/mg, σ in cm²/device, unless otherwise specified	Supply Voltage	Sample Size (Number Tested)
Power Devices:								
IRHLF87Y20	International Rectifier	1445, (15-001)	MOSFET	Trench	H: (LBNL2016Nov) JML	1039-MeV Ag (LET=48): SEB, SEGR. Last pass/first fail V_{DS}: 18/20V at 0, -1 V_{GS}; 16/18V at -2 V_{GS}; 14/16V at -3 V_{GS}.	V_{GS} = 0 V to -3 V in 1 V steps	12
Si7414DN	Vishay	n/a (16-030)	MOSFET	TrenchFET	H: (TAMU 2016Sep) MCC; P: (MGH 2016Oct) MCC; H: (LBNL 2016Nov) JML, MCC	Degradation from dose effects at all voltage settings and ion species. 548 MeV & 400 MeV Ar (LET=14&9.7): Last pass/first fail exhibited substantial part-part variability with failures as low as 30/33V. 283 MeV Ne (LET=2.7): 42/45V [15]	0 V_{GS}	15
SQJ431EP	Vishay	n/a (16-025)	MOSFET	TrenchFET	H: (TAMU 2016Sept) MCC	548 MeV Ar (LET=14): Pass at max rated V_{DS} = -200V. No dose effects.	0 V_{GS}	2
SMHF2812D	Crane Interpoint	1021 and 1214 (14-021)	DC/DC Converter	Hybrid	H: (TAMU 2016July) MCC	Destructive SEE observed in older LDC when biased at 35 V and 188 mA load on each output with 2127 MeV Au (LET = 86 MeV•cm²/mg). [16]	28 V, 35 V	6
CPM2-1200-0025B	CREE/Wolfspeed	1327, (13-069); FM113-16, (15-067)	MOSFET	SiC Gen 2 VDMOS	H: (TAMU_2016Apr) JML	466 MeV Ar (LET$_{SIC}$ = 9.3): At 0 V_{GS}, onset V_{DS} for latent gate degradation as a function of angle of incidence followed the cosine rule. Onset at 0°: 375 V. 566 MeV Cu (LET$_{SIC}$ = 24): At 0 V_{GS}, onset V_{DS} for gate-drain degradation = 200 V.	0 V_{GS}	3
Engineering Samples	GE	(16-042)	MOSFET	SiC	H: (TAMU 2016Sept) JML	Contact PI for information.	Various	Various
SOC/Processor/FPGA Devices:								
Jetson TX1	nVidia	n/a (16-038)	SOC	20nm CMOS	P: (MGH2016Oct) EW	SEU σ ~6.22x10⁻⁹ cm² at 200 MeV proton. [17]	19 V	1
Snapdragon 820	Samsung	n/a	SOC + DDR4	14nm LPP	H: (TAMU2016Sept) SG; P: (MGH2016Oct) SG	H: SOC (DDR4 not tested) SEFI LET_{th} ~ 1; $\sigma_{saturation}$ 3x10⁻⁶cm² (at LET=15); P: tested at 200 MeV: stuck bits at 1x10⁻¹⁰cm²/bit; SEFIs observed at 1x10⁻⁹cm² [18]	Defined by device board	4
RT4G150-CB1657	Microsemi	1548, 1629 (16-003, 16-032)	FPGA	65nm CMOS	H: (LBNL 2016Sept) (TAMU 2016Oct-Nov) (LBNL 2016Oct) MB	1 <SEU LET_{th} <1.8 [19] [20] [21] [22]	nominal	5
XC7K325T-1FBG900 Kintex K7	Xilinx	1349 (14-001)	FPGA	FPGA (28nm planar)	H: (TAMU 2016Oct-Nov) MB	SEU LET_{th} <0.07; SEL LET_{th} <8 [20] [21] [23] [24]	nominal	3
XCKU040-1LFFVA1156I Kintex-UltraScale	Xilinx	1509 (15-061)	FPGA	FPGA (20nm planar)	H: (TAMU 2016Oct) MB	SEU LET_{th} <0.07; SEL LET_{th} > 50 [25]	nominal	2
Memory Devices:								
H27QDG8Z2C8R-BCG	Hynix	608A (16-010)	3D NAND Flash	ONO Charge-trap and CMOS	H: (LBNL2016Aug) DC/TW	MLC-mode SEU: LET_{th} < 0.9 MLC-mode SEU: $\sigma_{saturation}$ = 1x10⁻¹⁰ cm²/bit (For checkerboard pattern to fluence of 1x10⁷/cm². Pattern and fluence dependencies exist [26].) SLC-mode SEU: 0.9 < LET_{th} < 3.5 SLC-mode SEU: $\sigma_{saturation}$ = 5x10⁻¹⁰ cm²/bit SEFI: 0.9 < LET_{th} < 3.5 Permanent Failure of Erase Circuitry: 31 < LET_{th} < 35 SEL: LET_{th} > 85	1.8 V	3
IMMX64M64D3DUS8AG-E125	Intelligent Memory	n/a (14-063)	DDR3	Bit-twinned ECC Memory	H: (TAMU 2016July; TAMU 2016Oct-Nov) MCC	SEFI LET_{th} < 1.8 MeV•cm²/mg (σ ~ 2×10⁻⁶ cm⁻²). SET LET_{th} and σ could not be found due to on-chip ECC. No destructive SEEs at maximum tested LET = 20.6 MeV•cm²/mg.	1.5 V	1
IMME128M64D3DUS8A G-E125	Intelligent Memory	n/a (14-064)	DDR3	ECC Memory	H: (TAMU 2016July) MCC	SEFI LET_{th} < 1.8 MeV•cm²/mg (σ ~ 3×10⁻⁷ cm⁻²). SET LET_{th} and σ could not be found due to on-chip ECC. No destructive SEEs at maximum tested LET = 21 MeV•cm²/mg.	1.5 V	1
HM628128	Hitachi	9249 (15-082)	SRAM	0.8um CMOS	P: (MGH 2016Oct) MCC	SEU σ ~1x10⁻⁷ cm² with 200 MeV proton.	5 V	1
Linear Devices:								
AD9257	Analog Devices	1450 (16-023)	ADC	180 nm CMOS	H: (LBNL2016July; 2016Aug) DC	SEL LET_{th} > 86; SEU LET_{th} < 3.5; SET LET_{th} <2.5; 1.8 < SEFI LET_{th} < 3.5 [27]	1.8 V_{dd}	3
LTC6268-10	Linear Technology	1433 (16-040)	Operational Amplifier	BiCMOS	H: (TAMU2016July; LBNL2016July) DC	SEL LET_{th} > 86; SET $\sigma_{saturation}$ = 1.5x10⁻³ cm²: Two types of SET were observed: SETs with a short duration on the order of microseconds, and SETs with long duration on the order of milliseconds. The majority of SETs have duration less than 7 µsec. [28]	2.5 V	7
LTC6103	Linear Technology	n/a (16-031)	Current Sense Amplifier	linear bipolar	H: (LBNL2016Aug) MJC	SEL LET_{th} > 86; SET LET_{th} < 3.5; SET $\sigma_{saturation}$ ~ 5x10⁻⁴ cm² Positive and negative going transients independent of input voltage. [29]	4 to 60 V in 14 V increments	4
Diodes:								
JANTX1N6843CCU3	Microsemi	1233 (16-006)	Schottky Diode	Si	H: (TAMU 2016March19) MCC	No failures or degradation observed at 100% of reverse voltage when irradiated up to 729 MeV Cu (LET = 20 MeV•cm²/mg). Degradation observed during beam run while biased beginning at 85% of reverse voltage, but all parameters remained within specification when irradiated with 1170 MeV Ag (LET = 44 MeV•cm²/mg). Degradation was also observed during beam run when biased at 95% of reverse voltage and irradiated with 1470 MeV Pr (LET = 60 MeV•cm²/mg), but parameters exceeded specification. Degradation and exceeded specification limits were also observed when biased at 65% of reverse voltage and irradiated with 1858 MeV Ta (LET = 79 MeV•cm²/mg). [30]	100 V	3
JANS1N6843CCU3	International Rectifier	1217 (16-006)	Schottky Diode	Si	H: (TAMU 2016March) MCC	No failures or degradation observed at 100% of reverse voltage when irradiated up to 1470 MeV Pr (LET = 60 MeV•cm²/mg). Catastrophic failure was observed at 95% of reverse voltage when irradiated with 1858 MeV Ta (LET = 79 MeV•cm²/mg). [30]	100 V	4
SBRT10U60D1	Diodes, Inc.	1523 (16-043)	Super Barrier Diode	Si	H: (LBNL 2016Nov) MCC	No failures observed at 50% of reverse voltage when irradiated with 1233 MeV Xe (LET = 59 MeV•cm²/mg). Catastrophic failure was observed at 75% of reverse voltage.	60 V	3
SBR1045D1	Diodes, Inc.	1034 (16-044)	Super Barrier Diode	Si	H: (LBNL 2016Nov) MCC	No failures observed at 75% of reverse voltage when irradiated with 1233 MeV Xe (LET = 59 MeV•cm²/mg). Catastrophic failure was observed at 100% of reverse voltage.	45 V	3
SBR160S23	Diodes, Inc.	A8 (16-045)	Super Barrier Diode	Si	H: (LBNL 2016Nov) MCC	No failures observed at 100% of reverse voltage when irradiated with 1233 MeV Xe (LET = 59 MeV•cm²/mg).	60 V	3
BZX84-A75	NXP Semiconductor	31 (16-046)	Zener Diode	Si	H: (LBNL 2016Nov) MCC	No failures observed at 100% of reverse voltage when irradiated with 1233 MeV Xe (LET = 59 MeV•cm²/mg).	75 V	3
BZX84C75	ON Semiconductor	N (16-047)	Zener Diode	Si	H: (LBNL 2016Nov) MCC	No failures observed at 100% of reverse voltage when irradiated with 1233 MeV Xe (LET = 59 MeV•cm²/mg).	75 V	3
HSMP-3810	Broadcom	U (16-048)	PIN Diode	Si	H: (LBNL 2016Nov) MCC	No failures observed at 100% of reverse voltage when irradiated with 1233 MeV Xe (LET = 59 MeV•cm²/mg).	100 V	3
BAS21-7-F	Diodes, Inc.	D4 (16-049)	Diode	Si	H: (LBNL 2016Nov) MCC	Degradation observed during beam run when biased at 100% of reverse voltage, but all parameters remained within specification when irradiated with 1233 MeV Xe (LET = 59 MeV•cm²/mg).	200 V	3
Miscellaneous Devices:								
ADV212	Analog Devices	1216 (13-051); 1220 (13-053)	Video Codec	180nm CMOS	H: (TAMU 2016Sept) TW	SEL LET_{th} < 1.3; SEFI LET_{th} < 1.3; 43 < Permanent Failure LET_{th} < 52 [31] [32]	Core: 1.5 V I/O: 2.5 V	3
KSW-2-46+	Mini-Circuits	1643 (17-004)	RF Switch	GaAs	L: (NRL 2017Feb) MCC	Worst case transients were ~1 V in amplitude and ~10 ns in duration. Transients did not result in changed states. No destructive events were observed.	-5 V	2
AD8138	Analog Devices	1540A (N/A)	ADC Driver	SiGe	L: (NRL 2016Sept) MCC	Worst case transients were ~200 mV in amplitude and several µs in duration or ~3.5V in amplitude and 1 µs in duration. No destructive events were observed.	±5 V	2
AD9364	Texas Instruments	1401 (15-071)	RF Transceiver	65 nm CMOS	H: (TAMU2016Mar) DC	SEL LET_{th} > 87 (at fluence of 6.7×10⁶ cm⁻²); SEFI LET_{th} < 2.8 [33]	3.3 V	1

As in our past workshop compendia of NASA Goddard Space Flight Center (GSFC) test results, each DUT has a detailed test report available online at http://radhome.gsfc.nasa.gov describing the test method, SEE conditions/parameters, test results, and graphs of data. The Test Results and Discussion section contains summaries of testing performed on a selection of featured parts.

Test Results and Discussion

LTC6268-10 Linear Technology Operational Amplifier

We irradiated 7 samples with 15 MeV/amu heavy ions at TAMU and with 10 MeV heavy ions at LBNL. The SEE test circuit was configured with a gain of 100 dB.

We found that the LTC6268-10 is susceptible to heavy ion-induced SET. We evaluated the SET characteristics for an input current of 10, 100, and 200 nA. The output trigger was set to 200 mV_{pp} to compensate for the level of facility background noise.

Fig. 1 shows the SET cross section vs. effective LET for various input currents. Fig. 2 shows a SET amplitude vs. duration distribution plot. The figure shows that the SETs can be generally divided into two categories: 1) SETs with a short duration on the order of microseconds, and 2) SETs with long duration on the order of milliseconds. The majority of SETs have duration less than 7 µsec. Fig. 3 shows an example of a worst case SET.

Fig. 4 shows a column bar chart of the SET count for small and large events at input currents of 10, 100, and 200 nA. The SET count generally increases with decreasing input current for both small and large events.

Furthermore, the number of small events increases significantly with decreasing input current. The SET count for small events is significantly higher at 10 nA input current, and the proportion of small to large events is enhanced at 10 nA relative to 100 and 200 nA.

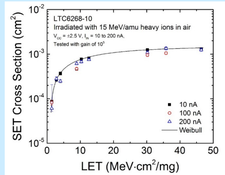

Fig. 1. SET cross section vs. effective LET for the LTC6268-10 irradiated with 15 MeV/amu heavy ions in air.

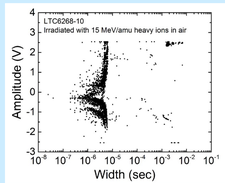

Fig. 2. SET amplitude vs. width plot (for all LETs) for the LTC6268-10 irradiated with 15 MeV/amu heavy ions in air.

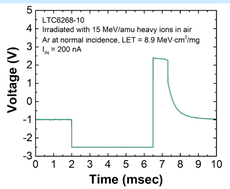

Fig. 3. SET characteristics for the LTC6268-10 (for all LETs) irradiated with 15 MeV/amu heavy ions in air.

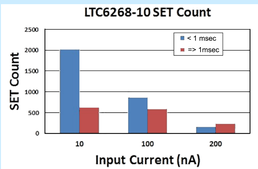

Fig. 4. SET count vs. input current for the LTC6268-10 irradiated with 15 MeV/amu heavy ions in air. The SETs are divided into two categories with respect to its duration: < 1 msec, and ≥ 1 msec. Data represents all LETs tested (Ne, Ar, Kr, and Au). The proportion of large and small SETs showed no clear dependence on LET.

Diode Failure Summary

In the 2016 "Compendium of Single Event Effects Results from NASA Goddard Space Flight Center," we presented the top-level results of the SEE testing of a variety of diodes. One of the diodes discussed was the Diodes, Inc. SBR20A300, which is a dual 300-V, 20-A super barrier diode. A decapsulated DUT is shown in Fig. 5 mounted on a daughtercard. Five of the SBR20A300s were irradiated at LBNL with 1233-MeV Xe, which has an LET of 58.8 MeV•cm²/mg. These parts experienced catastrophic failure when reverse biased at 225V or 300V (the parts were only biased at increments of 25% of the rated reverse voltage.) However, when biased at 50% of the rated reverse voltage, 150V, only charge collection was observed. Fig. 6 shows the reverse current during the beam run where the diode was reverse biased at 150V. When the SBR20A300 is reverse biased at 150V (50% of the rated reverse voltage), only charge collection is observed after the beam is turned on at time 0s.

The beam shutter was opened (beam was turned on) at time 0 s, and charge collection was immediately observed. When the shutter was closed (beam was turned off), the reverse current recovers to approximately the original value. After power was removed from the DUT, after the beam was turned off, the forward and reverse currents and voltages were measured to determine if any degradation occurred. No shifts were observed in any of these parameters. The reverse voltage on the same DUT was then increased by 25% to 225V and irradiated. Shortly after the beam was turned on, the reverse current begins to increase and then suddenly the current increases to the point where the anode and the cathode are shorted and the amount of reverse current is limited by the compliance settings on the power supply. This is shown in Fig. 7.

After the beam run was over, there were significant shifts in the electrical parameters. Fig. 8 shows the reverse current as a function of the reverse voltage, and while there was little shift from the pre-rad measurements after the part was irradiated while biased at 150V (50% of the rated reverse voltage), the part exceeded the specification for reverse current (10 µA) before the reverse voltage reached 1V, which is well below the specification of 300V. After the SBR20A300 is irradiated while biased at 150V there is effectively no change in the reverse current as a function of reverse voltage when compared to the pre-irradiation values. However, when the reverse current-reverse voltage sweep is measured after the part was irradiated while biased at 225V (75% of the rated reverse voltage), the specification for reverse current (maximum of 100 µA) was exceeded before the reverse voltage reached 1V, indicating that the anode and cathode were shorted.

After returning to Goddard, several of these parts were taken to the Parts Analysis Lab (NASA GSFC, Code 562) for failure analysis. The parts were photographed with a thermal infrared camera with a small reverse bias applied (Fig. 9). The bright white spot in the upper left corner of the die during the guard ring was quickly determined to be a failure location, and a second darker spot about halfway down the left side along the guard ring was also identified. These locations were then photographed with a high-magnitude optical microscope and these images can be seen in Figs. 10 and 11. Only the brighter, upper corner failure location will be discussed in this work. The DUT was then cross-sectioned at the location of this failure. Fig. 12 shows the location of the failure in cross-section. A large void is visible, as are cracks due to stress from the excessive that resulted from the heavy ion strike. There is also a large mound directly below the void that was created after the silicon melted and then reformed. A large void is observed from the displacement of molten silicon, as is a large mound-shaped region directly below the void. In addition, cracks are observed due to stress from the excess heat created by the heavy ion as it passed through the diode.

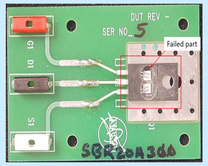

Fig 5. An example DUT of the SBR20A300 super barrier diode manufactured by Diodes, Inc. is mounted on a daughtercard for heavy-ion irradiation at LBNL.

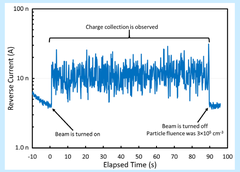

Fig 6. Charge collection is observed when reverse biased at 150V (50% of the rated reverse voltage).

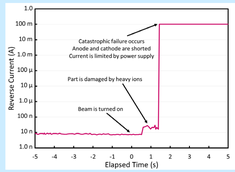

Fig 7. Reverse current increases and part experiences catastrophic failure when reverse biased at 225V (75% of the rated reverse voltage).

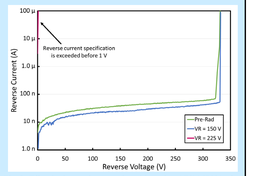

Fig 8. Effectively no change when biased at 150V (50% of the rated reverse voltage); anode and cathode were shorted when biased at 225V (75% of the rated reverse voltage).

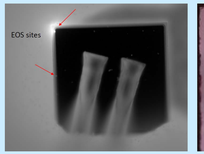

Fig 9. Infrared camera photograph reveals two locations showing elevated temperatures when a small bias is applied.

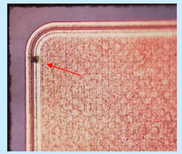

Fig 10. High-magnitude optical microscope photograph of the failure location shown in the thermal image in Fig. 9.

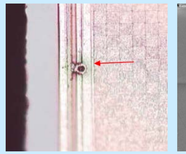

Fig 11. High-magnitude optical microscope photograph of the dimmer failure location in Fig. 9.

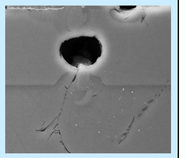

Fig 12. Cross-section of failure location shown in Figs. 9 and 10 reveals stress cracks and a large void.

Summary

We have presented current data from SEE testing on a variety of mainly commercial devices. It is the authors' recommendation that these data be used with caution. We also highly recommend that lot testing be performed on any suspect or commercial device.

Acknowledgment

This work was supported in part by the NASA Electronic Parts and Packaging (NEPP) Program, NASA Space Technology Mission Directorate Game Changing Technology Division, and NASA Flight Projects.

The authors gratefully acknowledge members of the Radiation Effects and Analysis Group who contributed to the test results presented here: Hak Kim, Anthony M. Phan, Donna J. Cochran, James D. Forney, Christina M. Seidleck, and Stephen R. Cox.

Special thanks go to Stephen P. Buchner and Dale McMorrow, Naval Research Laboratory for their excellent support of the laser testing.